

ELECTRON BEAM INDUCED IMPURITY ELECTRO-MIGRATION IN

UNINTENTIONALLY DOPED GaN

M. Toth*, K. Fleischer** and M. R. Phillips*

*Microstructural Analysis Unit, University of Technology, Sydney, PO Box 123, Broadway, NSW 2007, Australia, matthew.phillips@uts.edu.au

** On leave from Technical University of Berlin

Abstract

Electron beam induced electromigration of O_N^+ and H^+ impurities in unintentionally n-doped GaN was investigated using cathodoluminescence (CL) kinetics profiling, CL imaging of regions pre-irradiated with a stationary electron beam, and wavelength dispersive x-ray spectrometry (WDS). The presented results (i) illustrate induced impurity diffusion in wide bandgap semiconductors, (ii) provide experimental evidence for the $(V_{Ga}-O_N)^{2-}$ model of yellow luminescence in GaN with low Si content¹, (iii) confirm the roles of O in frequently reported bound exciton and donor-acceptor pair emissions and (iv) suggest the involvement of O_N^+ and hydrogenated gallium vacancies in a blue emission in autodoped GaN.

Introduction

CL is light emitted due to recombination of e-h pairs generated by energetic electrons. CL kinetics profiles can be obtained by recording the CL signal as a sample is irradiated with the electron beam in a scanning electron microscope (SEM). Electron beam irradiation of an uncoated semiconductor or insulator produces a positive region at the beam impact point due to a loss of charge through the emission of secondary electrons. The positive region (of <50nm) is followed by a negative region produced by the electrons injected into the sample². During electron beam irradiation CL intensity can change due to (i) diffusion of radiative or nonradiative centers in or out of the electron interaction volume, (ii) competitive recombination due to differences in recombination efficiencies between different luminescent centers, (iii) trapping of injected charge and consequent distortion of the interaction volume² and (iv) buildup of electron beam induced contamination on the sample surface and consequent CL absorption.

Experimental Procedure

The sample used in this study was an unintentionally n-doped 4 μ m epilayer of wurtzite GaN grown at 1040°C on a 25nm GaN buffer layer by metal-organic chemical vapor deposition. The buffer was grown at 550°C on a c-plane sapphire substrate. Trimethylgallium and ammonia were used as precursors. CL and WDS measurements were performed using an Oxford Instruments MonoCL2 scanning CL spectroscopy and imaging system and a Microspec WDS system both installed on a JEOL35C SEM with a liquid helium cold stage. The CL signal was dispersed by a 1200 lines/mm grating blazed at 500nm and detected using a Hamamatsu R943-02 peltier cooled PMT. Optical absorption measurements were performed using a Hitachi U3400 UV-VIS-NIR spectrometer. CL kinetics profiles were obtained by blanking the electron beam, driving the sample to a previously unirradiated region and by recording the CL signal as a function of time as the sample was irradiated with a stationary electron beam (“spot mode”). To minimize beam-induced effects during data acquisition, CL spectra and images were obtained using the minimum beam currents and dwell time (200 μ s per pixel) needed for satisfactory S/N

ratios. CL spectra have been corrected for system response. Noise in CL kinetics profiles and asymmetries in beam induced features in CL images are contributed to by a strong dependence of ion diffusion on the local charge trap density (impurity and defect concentration). The features discussed below represent typical, reproducible behavior.

CL spectroscopy of GaN

CL spectra obtained using a beam energy (E_b) of 15keV and beam currents (I_b) of 0.5nA at 300K and 0.14nA at 4K are shown in figure 1(a). The room temperature spectrum consist of a near-edge emission at 3.4eV and the yellow luminescence (YL) centered on 2.07eV (FWHM = 540meV). The liquid He spectrum contains a donor-bound exciton (DX) peak³ at 3.46eV (FWHM = 20meV) with a phonon replica at 3.39eV. The DX peak is contributed to by a free exciton (FX) emission not resolved as an individual peak in the spectrum³. A donor-acceptor pair (DAP) emission with 2 LO phonon replicas³ are observed at 3.25, 3.16 and 3.07eV respectively. A blue luminescence (BL) is positioned at approximately 2.8eV while the YL is centered at 2.24eV (FWHM = 450meV). The features below 1.75eV are second order peaks. The DAP emission has been reported to be associated with O donors⁴. Ripples in the BL and YL bands are caused by the microcavity effect⁵.

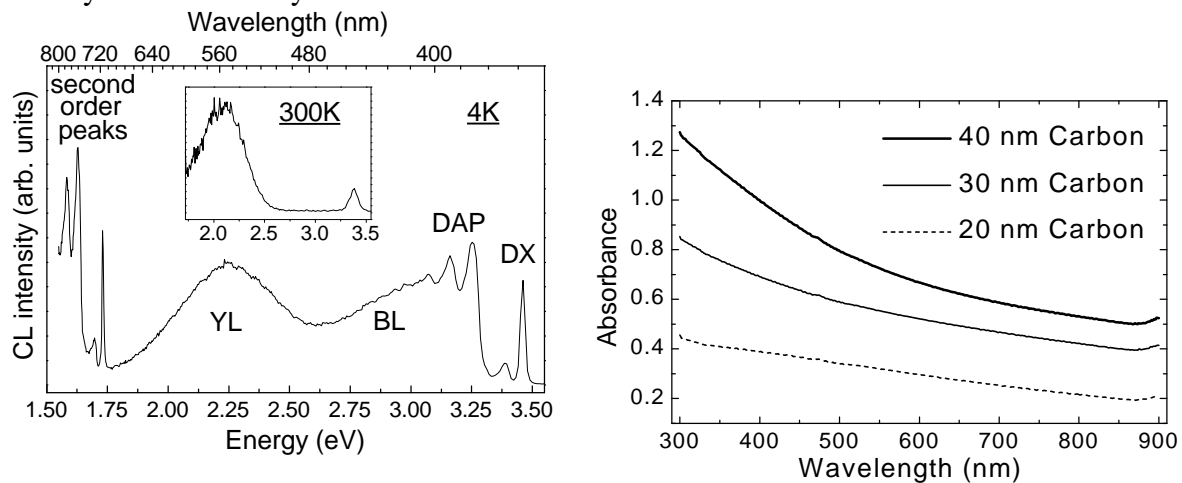


Figure 1. (a) CL spectra ($E_b=15\text{keV}$, corrected for system response) of autodoped GaN obtained at 4K ($I_b=0.14\text{nA}$, band pass=1nm) and 300K (inset, $I_b=0.5\text{nA}$, band pass=2.5nm). The high intensity of the second order peaks is a system response correction artifact. (b) Optical absorption spectra of 20, 30 and 40nm C films deposited under identical conditions.

YL has been attributed to a shallow donor-deep acceptor transition⁶. The most energetically favorable native deep acceptor in n-type GaN is the gallium vacancy (V_{Ga}^{3-}). V_{Ga}^{3-} can form a complex with the nearest neighbor O_{N}^+ and a less stable complex with the second nearest neighbor Si_{Ga}^+ . $(V_{\text{Ga}}-\text{O}_{\text{N}})^{2-}$ and $(V_{\text{Ga}}-\text{Si}_{\text{Ga}})^{2-}$ complexes have low formation energies and are expected to play significant roles in YL generation^{1,7}.

Electron beam irradiation in an SEM can induce a C contamination layer on the specimen surface¹¹. The contamination preferentially absorbs the blue end CL and hence modulates CL spectra and kinetics profiles. Optical absorption spectra of 20, 30 and 40nm C films are shown in figure 1(b). The observed decrease in the absorbance with increasing wavelength is used to explain some features of CL kinetics profiles presented in the following sections.

WDS kinetics of GaN

High concentrations of O_N^+ (approximately $10^{18} - 10^{20} \text{ cm}^{-3}$)¹³ can occur in n-type GaN, particularly in samples with low Si_{Ga}^+ content¹. To determine the dominant impurity in the sample, $O_{K\alpha}$ and $Si_{K\alpha}$ lines were measured using WDS. Si was not detected under any conditions. WDS spectra showing the $O_{K\alpha}$ and $N_{K\alpha}$ lines acquired in spot mode before and after a 30min irradiation are shown in figure 2(a). The spectra were acquired using a beam energy of 25keV and a beam current of 300nA to obtain a sufficiently strong $O_{K\alpha}$ signal. The $O_{K\alpha}$ peak increased and the $N_{K\alpha}$ decreased during the irradiation. The $N_{K\alpha}$ decay is caused by x-ray absorption in a C contamination layer induced on the sample surface by the electron beam¹¹. The $O_{K\alpha}$ increase is attributed to O_N^+ electro-diffusion from the surface and bulk towards the negative region of the electron interaction volume.

To verify that the $O_{K\alpha}$ increase is not related to the contamination layer, the spot mode $O_{K\alpha}$ and $C_{K\alpha}$ kinetics profiles shown in figure 2(b) were acquired from the sample. The $C_{K\alpha}$ intensity increased at a faster rate and, unlike the $O_{K\alpha}$, saturated after approximately 1400s. Oxygen contamination from residual gaseous O_2 is unlikely, as the SEM chamber pressure was approximately 2×10^{-6} Torr during irradiation experiments and (ii) the chamber was vented with dry nitrogen.

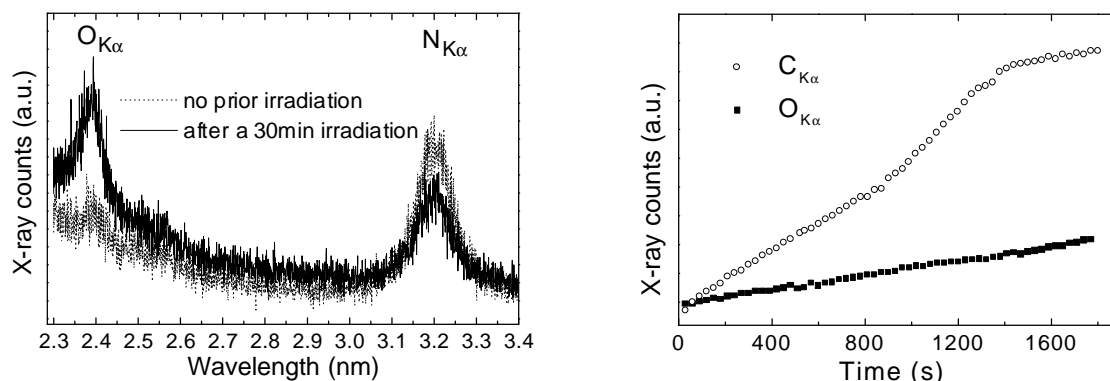


Figure 2. Qualitative WDS analysis of autodoped GaN (spot mode, $E_b=25\text{keV}$, $I_b=300\text{nA}$). (a) raw WDS spectra showing the $O_{K\alpha}$ and $N_{K\alpha}$ lines before and after a 30min irradiation, (b) $O_{K\alpha}$ and $C_{K\alpha}$ kinetics profiles. Si was not detected in the sample.

CL kinetics at room temperature

Room temperature CL kinetics profiles of the 3.4eV, BL and YL emissions are shown in figure 3(a). CL images of a region pre-irradiated using a stationary electron beam acquired using the above emissions are shown in figure 4. The room temperature kinetics profiles in figure 3(a) are dominated by the effects of H^+ and O_N^+ diffusion into and within the electron interaction volume. H^+ and O_N^+ impurities diffuse from the positive, near-surface region into the negative region of the interaction volume. The H^+ ions are most likely to originate at hydrogenated gallium vacancies and dangling bonds at the surface since interstitial hydrogen acts as an acceptor and has a high formation energy in n-type GaN⁸. The concentration of hydrogenated gallium vacancies hence decreases near the surface and increases in the bulk due to H^+ re-capture. Up to four H^+ ions can be incorporated at a gallium vacancy¹². H^+ causes the vacancy energy levels to split and shift towards the valence band¹². Outside the interaction volume,

O-related bonds are broken by short wavelength (UV) CL and O_N^+ impurities diffuse towards the negative region of the interaction volume.

At 25keV most of the detected BL and YL emissions originate approximately 300nm below the surface where the e-h pair generation rate maximizes¹⁰. Self-absorption of the near-edge emission causes most of the detected 3.4eV signal to be generated approximately 80nm below the surface¹⁰, in the vicinity of the H depleted region. Radiative recombination in the H depleted region is reduced by (competitive) nonradiative surface recombination. In figure 3(a), O_N^+ diffusion causes the increase in the 3.4eV and BL emissions over the first 30s of irradiation and the long term increase in YL intensity. The 3.4eV intensity increases because of competitive recombination with YL; O_N^+ diffusion reduces the $(V_{Ga}-O_N)^{2-}$ complex contribution to YL generation in the vicinity of the positive near-surface region where most of the detected 3.4eV signal originates. The YL intensity increases because O_N^+ diffuses from the positive near-surface layer and from outside the interaction volume into the region where YL generation maximizes. The O rich region is seen as the large bright features in the CL images in figure 4. The dark contrast in the center each oxygen rich region appears when the 3.4eV emission starts to decrease (after 30s in figure 3(a)). This contrast and the decay in the 3.4eV kinetics profile are caused by accumulation of a C contamination layer and consequent CL absorption at the sample surface around the beam impact point. The C absorption effect is most pronounced at 3.4eV and decreases with increasing CL wavelength (BL and YL), in consistence with the C absorption spectra in figure 1(b).

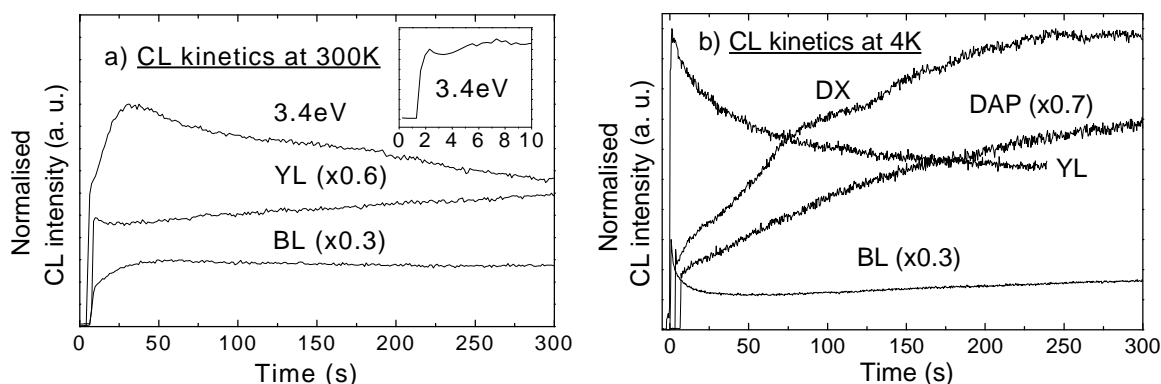


Figure 3. CL kinetics ($E_b=15\text{keV}$) of (a) 3.4eV, BL and YL emissions at 300K ($I_b=3\text{nA}$) and (b) DX, DAP, BL and YL emissions at 4K ($I_b=6\text{nA}$). The inset in (a) shows detail of the first 10s of the 3.4eV emission obtained using a lower electron dose ($I_b=1.2\text{nA}$).

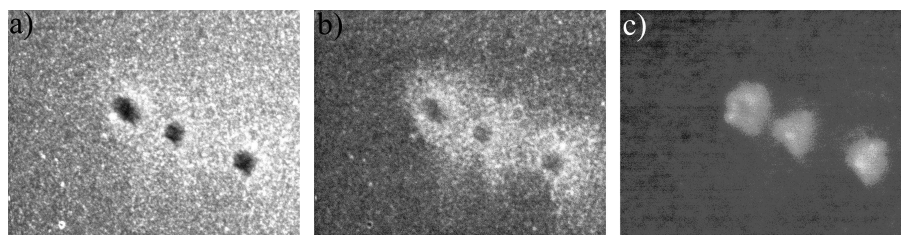


Figure 4. CL images ($T=300\text{K}$, $E_b=15\text{keV}$, $I_b=0.8\text{nA}$, horizontal field width = $95\mu\text{m}$) of a region pre-irradiated in 4 places using a stationary electron beam. The images were acquired using the: (a) 3.4eV, (b) BL and (c) YL emissions. Each spot irradiation was performed for approximately 10min ($I_b=5\text{nA}$).

H^+ diffusion causes the initial rapid, short lived decay of the 3.4eV (inset of figure 3(a)) and YL emission intensities. The 3.4eV decay reflects competitive recombination with YL centers activated by H^+ removal from gallium vacancies near the surface. The extent of the H^+ diffusion effect in spot mode kinetics profiles was found to vary across the sample due to a heterogeneous H^+ distribution in the sample. The variations in H concentration are probably caused by impurity congregation at extended defects and by deviations from thermodynamic equilibrium conditions during growth.

Electro-diffusion of both H^+ and O_N^+ into the negative region of the interaction volume, where most of the BL and YL signals are generated, causes the BL intensity to increase (figure 3(a)). We suggest a transition from a hydrogenated gallium vacancy to O_N^+ as a potential recombination path for BL generation. Under this assumption, the initial rapid increase in BL due to H^+ diffusion is caused by (i) effective creation of BL centers due to H passivation of gallium vacancies and (ii) a reduction in the concentration of competitive YL centers in the region where a majority of the BL signal is generated. The BL intensity maximizes after approximately 30s of irradiation and slowly decays due to BL absorption in the C contamination layer.

CL kinetics at base temperature

CL kinetics profiles of the DX, DAP, BL and YL emissions obtained at 4K are shown in figure 3(b). CL images obtained at 4K using the DX, DAP, BL and YL emissions after a 700s spot mode irradiation are shown in figure 5.

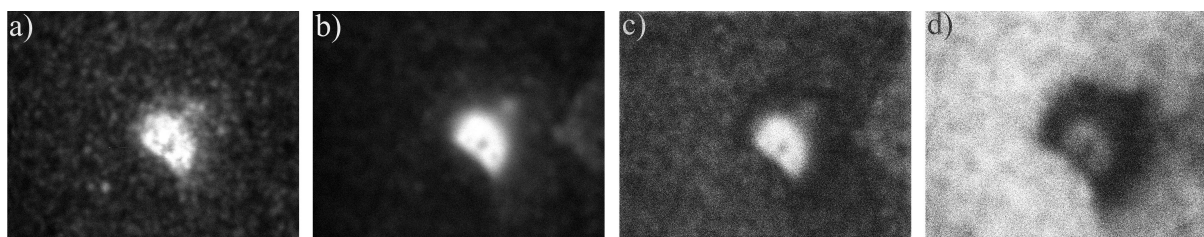


Figure 5. CL images ($T=4K$, $E_b=15keV$, $I_b=0.2nA$, horizontal field width = $42.5\mu m$) of a region irradiated in spot mode ($I_b=6nA$) for 700s acquired using the: (a) DX, (b) DAP, (c) BL and (d) YL emissions.

At 4K the kinetics profiles change at lower rates and the impurity diffusion effected regions in CL images are smaller than at 300K due to a reduction in the thermal energy of the sample. The base temperature kinetics profiles differ from their room temperature counterparts due to the presence of the DX and DAP emissions. The DX and DAP emissions are not present at 300K due to thermal ionization of O_N . The DX and DAP kinetics profiles increase during irradiation because of O_N^+ diffusion into the negative region of the interaction volume. The generation profiles of the detected DX and FX signals maximize approximately 80nm below the surface due to self-absorption. The exponential nature of self-absorption of near-edge luminescence limits the O_N^+ diffusion contribution to the increase in DX intensity due to the nonlinear relationship between O_N^+ concentration in the negative region of the interaction volume and the measured increase in DX intensity. The apparent increase in DX intensity is contributed to by the FX emission which increases in the vicinity of the H^+ and O_N^+ depleted near-surface region due to a reduction in the concentration of competitive DX, DAP, YL and BL centers. The increase in DAP intensity due to O_N^+ diffusion is consistent with the suggestion that O_N^+ is the donor is involved in the DAP transition⁴. The rapid decrease in BL and YL intensities

during irradiation at 4K is probably caused by competitive recombination with DAP, DX and FX centers.

At 4K, the O_N^+ diffusion effected regions are small enough and the S/N ratio in the CL images is sufficiently high to resolve an O_N^+ depleted region around the O_N^+ enriched region in the BL and YL images. The dark contrast (figure 5(c) and (d)) indicates where the surplus O_N^+ has diffused from. The absence of a dark ring in the DX image is caused by an increase in the FX emission in the O_N^+ depleted region. Its absence in the DAP image can be explained by the acceptor distribution, assuming that the acceptor concentration is much lower than that of O_N^+ . This assumption is plausible in light of the low O_N^+ and $(V_{Ga}-O_N)^{2-}$ formation energies in n-type GaN^{1,7}. The DAP center concentration is hence governed by the concentration of the (negative) acceptors which diffuse away from the negative region of the interaction volume at an apparently low rate. The acceptor involved in the DAP transition has been suggested to be C^4 , consistent with first principles calculations which show the C_N^- shallow acceptor to be the most energetically stable C state in n-type GaN¹.

Conclusion

Time resolved CL and WDS analysis of autodoped GaN was used to provide experimental evidence for the $(V_{Ga}-O_N)^{2-}$ model of yellow luminescence in GaN with low Si content¹, confirm the roles of O_N^+ in frequently reported bound exciton and donor-acceptor pair emissions and to suggest the involvement of O_N^+ and hydrogenated gallium vacancies in a blue emission in autodoped GaN.

We gratefully acknowledge Dr G. Li and Dr J. Zou for providing the sample used in this study.

References

1. J. Neugebauer and C. G. Van de Walle, Appl. Phys. Lett. 69 (4), 503 (1996).
2. J. Cazaux, J. Appl. Phys. 59 (5), 1418 (1986).
3. J. W. Orton and C. T. Foxon, Rep. Prog. Phys. 61, 1 (1998).
4. M. Leroux, B. Beaumont, N. Grandjean, P. Lorenzini, S. Haffouz, P. Vennegues, J. Massies and P. Gibart, Mat. Sc. & Eng. B 50, 97 (1997).
5. K. Knobloch, P. Perlin, J. Krüger, E. R. Weber, and C. Kisielowski, MRS Internet Journal of Nitride Semiconductor Research 3, 4 (1998).
6. P. Perlin, T. Suski, H. Teisseyre, M. Leszczynski, I. Grzegory, J. Jun, S. Porowski, P. Boguslawski, J. Bernholc, J. C. Chervin, A. Polian and T. D. Moustakas, Phys. Rev. Lett. 75 (2), 296 (1995).
7. T. Mattila and R. M. Nieminen, Phys. Rev. B 55 (15), 9571 (1996).
8. J. Neugebauer and C. G. Van de Walle, Phys. Rev. Lett. 75 (24), 4452 (1995).
9. M. Toth and M. R. Phillips, Scanning, (20), 425 (1998).
10. K. Fleischer, M. Toth, M. R. Phillips, J. Zou, G. Li and S. J. Chua, submitted for publication.
11. J. I. Goldstein, D. E. Newbury, P. Echlin, D. C. Joy, A. D. Romig, Jr., C. E. Lyman, C. Fiori and E. Lifshin, *Scanning Electron Microscopy and Microanalysis*, 2nd ed. (Plenum Press, New York and London, 1992), p. 514.
12. C. G. Van de Walle, Phys. Rev. B 56 (16), 10020 (1997).
13. G. Popovici, W. Kim, A. Botchkarev, H. Tang and H. Morkoc, Appl. Phys. Lett. 71 (23), 3385 (1997)